Synthesis and Photodynamic Effect of New Highly Photostable Decacationically Armed [60]- and [70]Fullerene Decaiodide Monoadducts to Target Pathogenic Bacteria and Cancer Cells

Min Wang,[†] Liyi Huang,[‡,§] Sulbha K Sharma,[‡] Seaho Jeon,[†] Sammaiah Thota,[†] Felipe F Sperandio,[‡,§,ξ,ɣ] Suhasini Nayka,[‡] Julie Chang,[‡,¥] Michael R. Hamblin,[*,‡,§,¥] and Long Y. Chiang[*,†,ǂ]

[†] Department of Chemistry, Institute of Nanoscience and Engineering Technology, University of Massachusetts, Lowell, MA 01854, United States

[‡] Wellman Center for Photomedicine, Massachusetts General Hospital, Boston, MA 02114, United States

[§] Department of Dermatology, Harvard Medical School, Boston, MA 02115, United States

[ξ] School of Dentistry, University of Sao Paulo, 05508-000, Brazil

[ɣ] CAPES Foundation, Ministry of Education of Brazil, Brasília, DF 70040-020, Brazil

[¥] Department of Chemistry, Harvard University, Cambridge, MA 02138, United States

[¥] Harvard–MIT Division of Health Sciences and Technology, Cambridge, MA 02139, United States

[ǂ] Department of Laboratory Medicine and Pathobiology, University of Toronto, Toronto, ON M5S 1A8, Canada

Supporting Information

Scheme S1. The carbon and proton number assignment for ^{1}H NMR spectra in Figures S3 and S4.

Figure S1. Infrared spectra of (a) C_{60}[>M(*t*-Bu)$_2$] **3**, (b) precursor arm M($C_3N_6^+C_3H)_2$, (c) C_{60}[>M($C_3N_6^+C_3H)_2$] **6**, (d) C_{60}[>M($C_3N_6^+C_3)_2$] **1**, and (e) C_{60}[>M($C_3N_6^+C_3)_2$] **1'**.

Figure S2. Infrared spectra of (a) C_{70}, (b) C_{70}[>M(*t*-Bu)$_2$] **4**, (c) precursor arm M($C_3N_6^+C_3H)_2$, (d) C_{70}[>M($C_3N_6^+C_3H)_2$] **7**, (e) C_{70}[>M($C_3N_6^+C_3)_2$] **2**, and (f) C_{70}[>M($C_3N_6^+C_3)_2$] **2'**.

Figure S3. ^{1}H NMR spectra of N_5C_3-NH_2, $C_3N_6C_3$-OH **5**, C_{60}[>M($C_3N_6^+C_3H)_2$] **6**, and C_{60}[>M($C_3N_6^+C_3)_2$] (**1** and **1'**) with peak assignments of all protons in the corresponding structures shown in Scheme S1.

Figure S4. ^{1}H NMR spectra of N_5C_3-NH_2, $C_3N_6C_3$-OH **5**, C_{70}[>M($C_3N_6^+C_3H)_2$] **7**, and C_{70}[>M($C_3N_6^+C_3)_2$] (**2** and **2'**) with peak assignments of all protons in the corresponding structures shown in Scheme S1.

Figure S5. ^{13}C NMR of (a) $C_{60}[>M(t\text{-}Bu)_2]$ **3** in $CDCl_3{-}CS_2$, (b) $C_{60}[>M(C_3N_6^+C_3H)_2]$ **6** in $CDCl_3{-}CS_2{-}$DMSO-d_6, and (c) $C_{60}[>M(C_3N_6^+C_3)_2]$ **1'** in $CDCl_3{-}CS_2{-}$DMSO-d_6.

Figure S6. ^{13}C NMR spectra of (a) $C_{70}[>M(t\text{-}Bu)_2]$ **4** in $CDCl_3/CS_2$, (b) decacationic $C_{70}[>M(C_3N_6^+C_3H)_2]$ **7** in $CDCl_3/CS_2$/DMSO-d_6 , and (c) decacationic $C_{70}[>M(C_3N_6^+C_3)_2]$ **2'** in $CDCl_3/CS_2$/DMSO-d_6.

Figure S7. MALDI−TOF mass spectra (a) and (b) of decacationic $C_{70}[>M(C_3N_6^+C_3)_2]$ **2** under different laser intensity using sinapic acid as the matrix, showing molecular ion mass (M^+) at *m/z* 3340.

Figure S8. Structural elucidation of fragmented ion mass peaks in the MALDI−TOF mass spectra (Figures S7a and S7b) of $C_{70}[>M(C_3N_6^+C_3)_2]$ **2**.

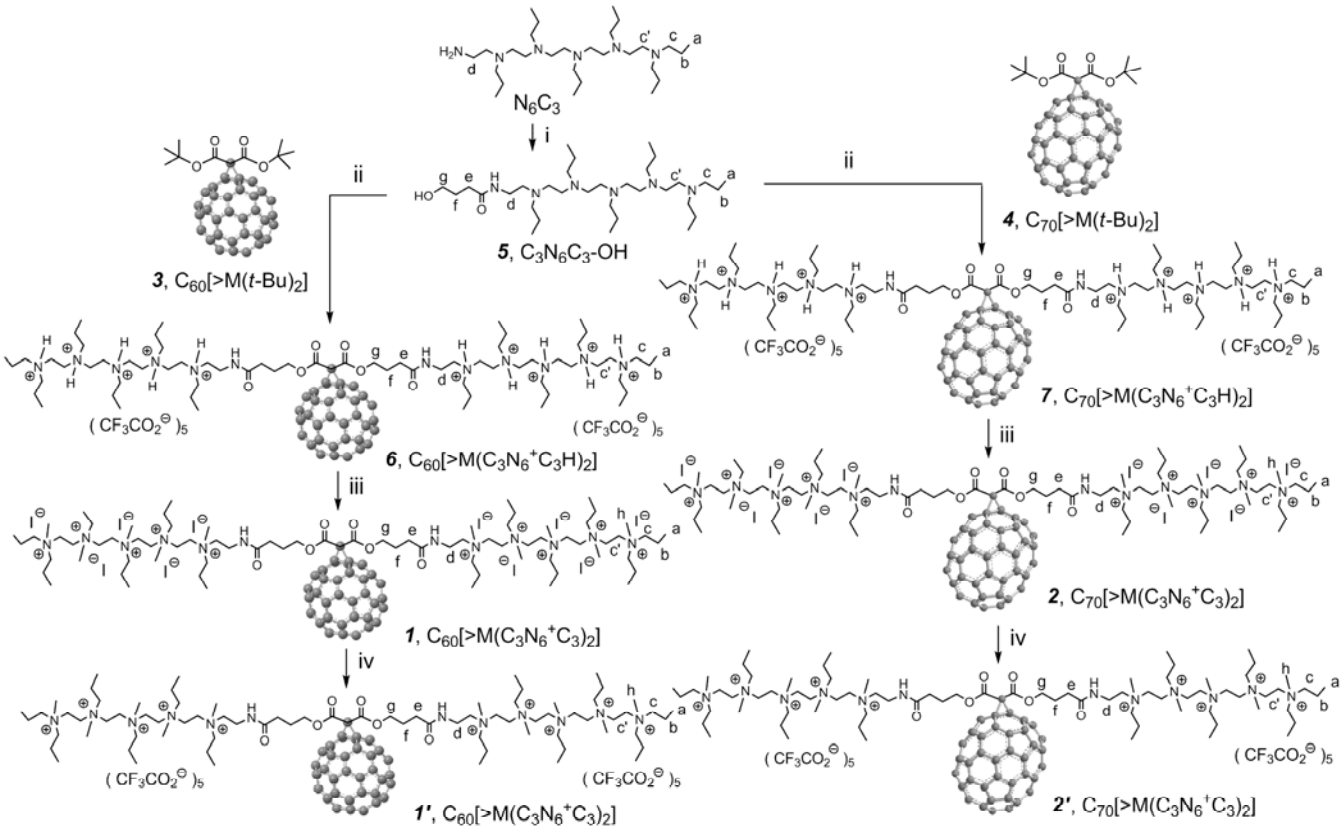

Scheme S1. The carbon and proton number assignment for ^{1}H NMR spectra in Figures S3 and S4.

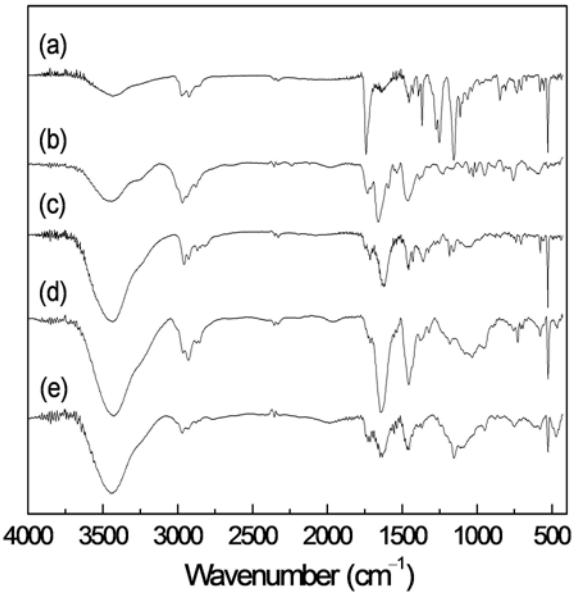

Figure S1. Infrared spectra of (a) C_{60}[>M(*t*-Bu)$_2$] **3**, (b) precursor arm M($C_3N_6^+C_3H)_2$, (c) C_{60}[>M($C_3N_6^+C_3H)_2$] **6**, (d) C_{60}[>M($C_3N_6^+C_3)_2$] **1**, and (e) C_{60}[>M($C_3N_6^+C_3)_2$] **1'**.

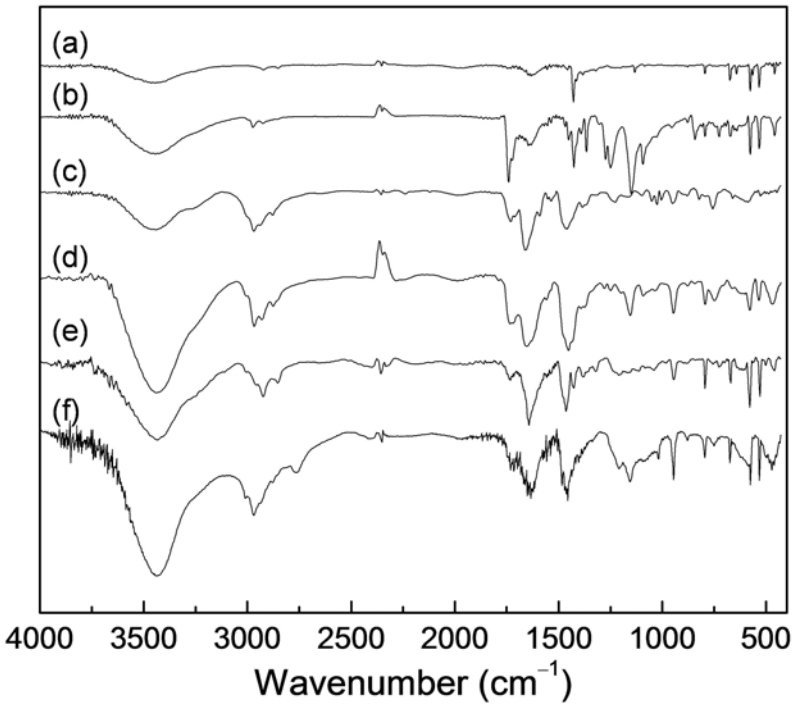

Figure S2. Infrared spectra of (a) C_{70}, (b) C_{70}[>M(*t*-Bu)$_2$] **4**, (c) precursor arm M($C_3N_6^+C_3H)_2$, (d) C_{70}[>M($C_3N_6^+C_3H)_2$] **7**, (e) C_{70}[>M($C_3N_6^+C_3)_2$] **2**, and (f) C_{70}[>M($C_3N_6^+C_3)_2$] **2'**.

FT-IR spectrum of C_{60}[>M(*t*-Bu)$_2$] **3** (Fig. S1a) showed a clear strong malonyl ester carbonyl (−C=O) vibrational absorption band centered at 1741 cm^{-1}. Peaks at 2924 and 2972 cm^{-1} are assigned to the stretching absorption band of aliphatic −C-H. Anti-symmetric deformations of −CH_3 groups and scissor vibrations of −CH_2 groups appeared as medium intensity bands centered around 1454 cm^{-1}, while symmetric deformations of CH_3 groups exhibited the absorption around 1367 cm^{-1}. A strong broad band at 1252 cm^{-1} was assigned to the asymmetric stretching vibrations of −C-C(=O)-O− moieties [*i.e*. mixed stretching vibrations of −C(=O)-O− and –C-C(=O)−], while the strong band centered at 1155 cm^{-1} is arising from the C(C_{60})-C-C(=O)− deformations, rocking −CH_3 vibrations, and –C-O-R (R = *t*-Bu) stretching vibrations. The sharp characteristic band at 527 cm^{-1} is assigned to the characteristic absorption of a half-cage moiety of C_{60}. Spectroscopic agreements of C_{60}[>M($C_3N_6^+C_3H$)$_2$] **6** (Fig. S1c) with the combination of that of the precursor arm **5** as di($C_3N_6C_3$-O-yl)malonate trifluoroacetate salt, M($C_3N_6^+C_3H$)$_2$ (Fig. S1b), with a strong peak at 1622 cm^{-1} assigned to the absorption of amide carbonyl –NH-C(=O)−, and the characteristic absorption band of a half-C_{60} cage moiety at 526 cm^{-1} gave the evidence of the transesterification product of **3**. Methyl quarternization of C_{60}[>M($C_3N_6C_3$)$_2$], having tertiary penta(ethylamino) arms, to C_{60}[>M($C_3N_6^+C_3$)$_2$] **1** with iodide salts and the corresponding **1'** with trifluoroacetate salts showed retention of the most of IR absorption bands (Figs.S1d and S1e, respectively), except the shift of –NH-C(=O)− band to 1641 cm^{-1} and a new broad band at 1000−1200 cm^{-1}, corresponding to the absorption of a number of quarternary −C-N$^+$-C− bonds. These results provided a good agreement of the product structure of **1**.

In the case of di(*tert*-butyl)[70]fullerenyl malonate C_{70}[>M(*t*-Bu)$_2$] **4** (Fig. S2b), rather similar features in characteristic absorption peak profiles with those of **3** were observed, including strong ester carbonyl (−C=O) vibrational absorption band centered at 1720 and 1741 cm^{-1}, the asymmetric stretching vibrations of –C-C(=O)-O− moieties [*i.e*. mixed stretching vibrations of −C(=O)-O− and –C-C(=O)−], at 1250 cm^{-1}, and the strong band of C(C_{60})-C-C(=O)− deformations and –C-O-R (R = *t*-Bu) stretching vibrations centered at 1150 cm^{-1}, contributed from the malonate addend moiety. Interestingly, four characteristic absorption bands of C_{70} (Fig. S2a) centered at 794, 671, 577, 532, and 458 cm^{-1} were clearly detected for **4** revealing a monoadduct structure that excludes the possible bismalonate products (with an additional malonate addend attaching at the α-bond of the opposite pole). Similarly,

spectroscopic agreements of $C_{70}[>M(C_3N_6^+C_3H)_2]$ **7** (Fig. S2d) with the combination of that of the precursor arm **5** as di($C_3N_6C_3$-O-yl)malonate trifluoroacetate salt, $M(C_3N_6^+C_3H)_2$ (Fig. S2c), with a strong peak at 1647 cm^{-1} assigned to the absorption of amide carbonyl –NH-C(=O)−, and the characteristic absorption bands of C_{70} cage moiety centered at 796, 582, 536, and 469 (br) cm^{-1} gave the evidence of the transesterification product of **4**. Methyl quarternization of $C_{70}[>M(C_3N_6C_3)_2]$, having tertiary penta(ethylamino) arms, to $C_{70}[>M(C_3N_6^+C_3)_2]$ **2** with iodide salts and the corresponding **2'** with trifluoroacetate salts showed retention of the most of IR absorption bands (Figs.S2e and S2f, respectively), except the shift of –NH-C(=O)− band to 1642 cm^{-1} a new broad band at 1010−1210 cm^{-1}, corresponding to the absorption of a number of quarternary –C-N^+-C− bonds. Sharp characteristic absorption bands of C_{70} cage moiety centered at 794, 671, 579, 530, and 459 (w) cm^{-1} were clearly detectable for **2**. These results provided a good agreement of the product structure of **2**.

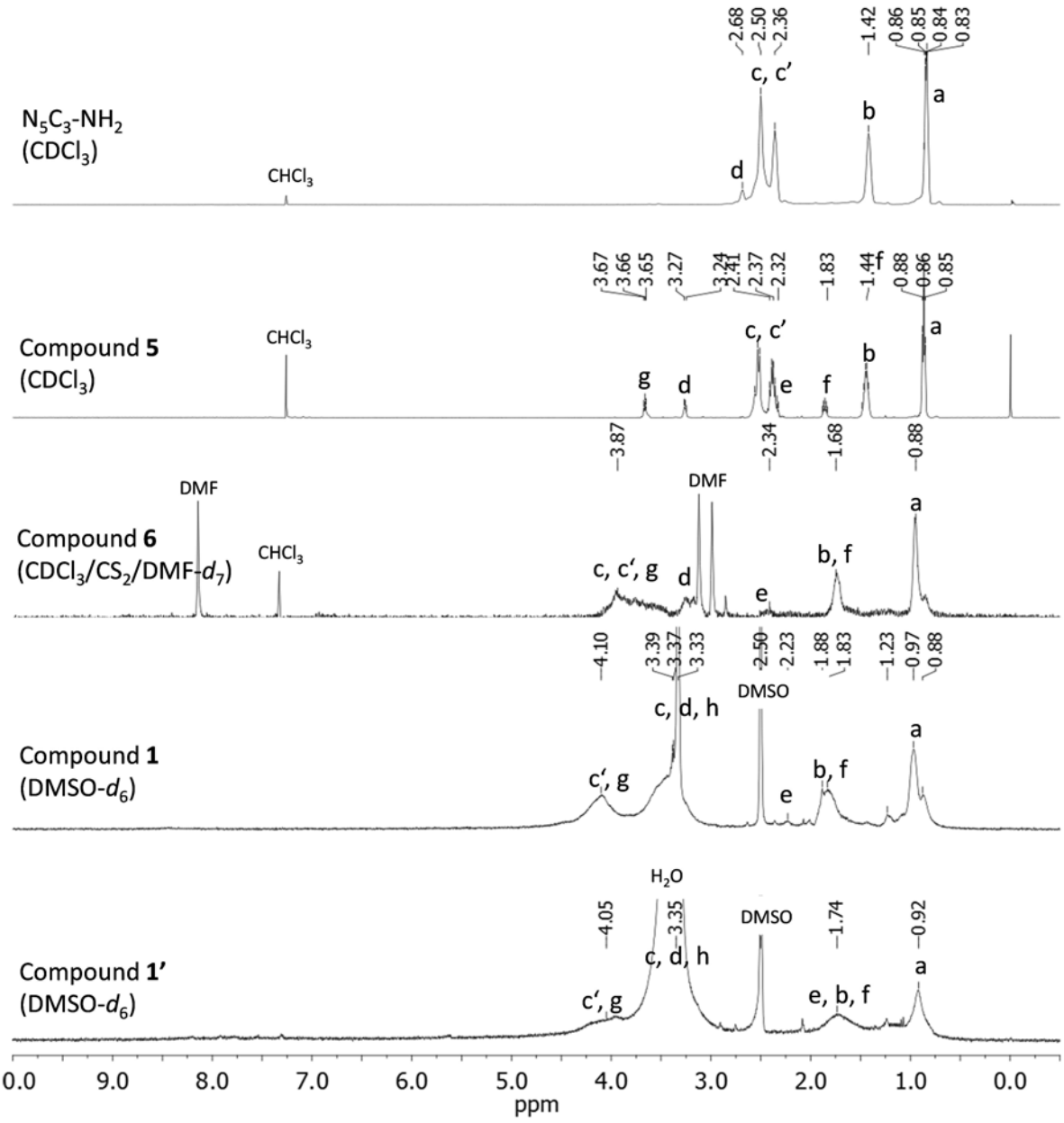

Figure S3. ^{1}H NMR spectra of N_5C_3-NH_2, $C_3N_6C_3$-OH **5**, $C_{60}[>M(C_3N_6^{+}C_3H)_2]$ **6**, and $C_{60}[>M(C_3N_6^{+}C_3)_2]$ (**1** and **1'**) with peak assignments of all protons in the corresponding structures shown in Scheme S1.

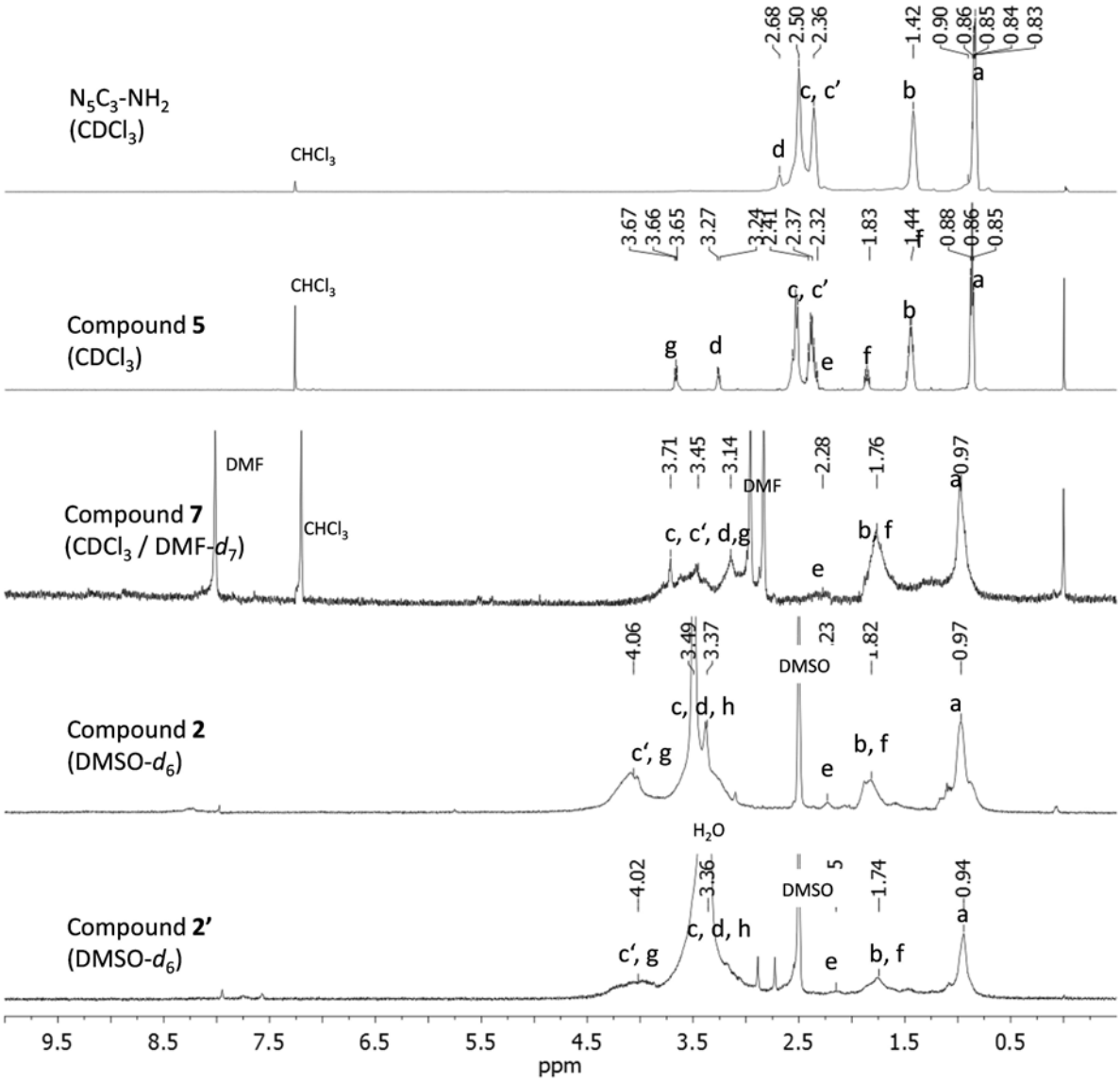

Figure S4. ^{1}H NMR spectra of N_5C_3-NH_2, $C_3N_6C_3$-OH **5**, C_{70}[>M($C_3N_6^+C_3H)_2$] **7**, and C_{70}[>M($C_3N_6^+C_3)_2$] (**2** and **2'**) with peak assignments of all protons in the corresponding structures shown in Scheme S1.

All proton peaks of compounds **5**, **6**, **1** and **1'** (Figure S3) were assigned with the corresponding proton numbers indicated on the compound structures shown in Scheme 1. Clear chemical shift assignment of all protons in the structure 4-hydroxy-[*N,N',N,N,N,N*-hexapropyl-hexa(aminoethyl)butanamide $C_3N_6C_3$-OH **5** was used to correlate the chemical shift changes of

C_{60}[>M($C_3N_6^+C_3H)_2$] **6** and C_{60}[>M($C_3N_6^+C_3)_2$] (**1** and **1'**) upon functional transformation from **5**. Accordingly, we assigned the peak at δ 3.27 (H_d) of **5** to the chemical shift of methylene protons of –C**H**$_2$-NH_2 and two peaks at δ 3.66 (H_g) and 1.83 (H_f) to methylene protons of −C**H**$_2$-OH and –CO-CH_2-C**H**$_2$-CH_2-OH, respectively. Transesterification reaction of C_{60}[>M(*t*-Bu)$_2$] **3** with **5** to C_{60}[>M($C_3N_6^+C_3H)_2$] **6** resulted in the introduction of protonated quaternary amine arm in the structure that caused a large down-fielded shift of chemical shifts (more than 1.0 ppm) of all *N*-attached ethyleneamino –C**H**$_2$– protons at δ 2.68–2.32 to δ 3.32−4.10 (H_c and $H_{c'}$) for quaternary ammonium methylene protons (–N^+-CH_2–), with the overlap of carboxylated methylene protons −C(=O)-O-C**H**$_2$− (H_g) at δ 4.0−4.25, as a broad band. The chemical shift of amidyl methylene protons (H_d) −C(=O)-NH-C**H**$_2$− was found to be δ 3.11−3.20 as multiplet peaks. Chemical shifts of all methyl or methylene proton peaks of C**H**$_3$-CH_2-CH_2-N−, CH_3-C**H**$_2$-CH_2-N−, and –CO-CH_2-C**H**$_2$-CH_2-OH were down-field shifted to δ 0.88 (H_a), δ 1.68 (H_b and H_f), and δ 2.34 (H_e), respectively. Upon the methyl quaternization to C_{60}[>M($C_3N_6^+C_3)_2$] (**1** and **1'**), additional methyl protons (H_h, –N^+-C**H**$_3$) increased the proton integration ratio at the region of δ 3.10−4.43. The chemical shift of all other protons remained in the similar corresponding range as those of **6**.

Nearly identical chemical shifts as those of Fig. S3 were made for assignments of all proton peaks of C_{70}[>M($C_3N_6^+C_3H)_2$] **7** and C_{70}[>M($C_3N_6^+C_3)_2$] (**2** and **2'**), as shown in Fig. S4, except a slight shift of chemical shifts of all methyl or methylene proton peaks in the moieties of C**H**$_3$-CH_2-CH_2-N−, CH_3-C**H**$_2$-CH_2-N−, and –CO-CH_2-C**H**$_2$-CH_2-OH to δ 0.97 (H_a), δ 1.76 (H_b and H_f), and δ 2.28 (H_e), respectively. Upon the methyl quaternization to C_{70}[>M($C_3N_6^+C_3)_2$] (**2** and **2'**), additional methyl protons (H_h, –N^+-C**H**$_3$) increased the proton integration ratio at the region of δ 3.10−4.43. The chemical shift of all other protons remained in the similar corresponding range as those of **7**.

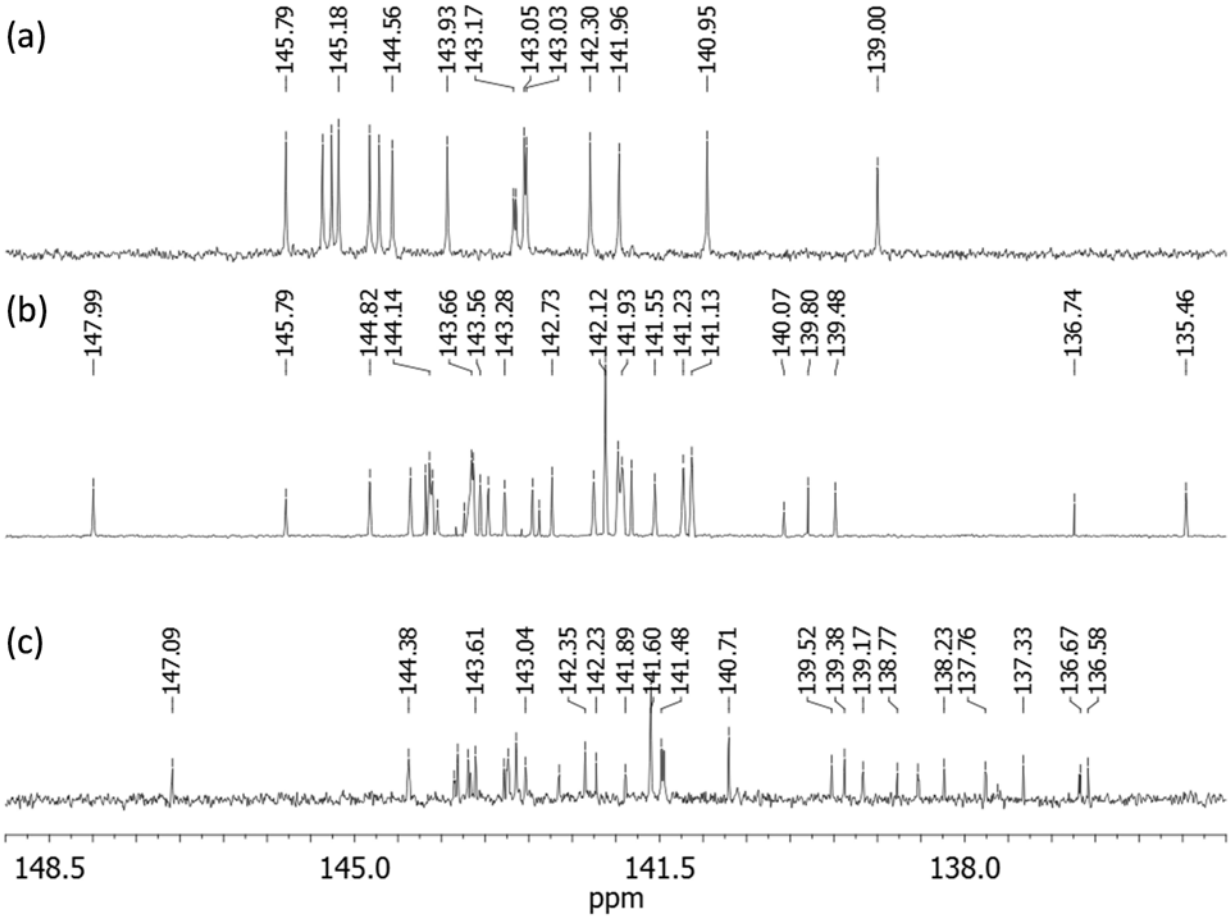

Figure S5. ^{13}C NMR of (a) C_{60}[>M(*t*-Bu)$_2$] **3** in $CDCl_3$−CS_2, (b) C_{60}[>M($C_3N_6^+C_3H$)$_2$] **6** in $CDCl_3$−CS_2−DMSO-d_6, and (c) C_{60}[>M($C_3N_6^+C_3$)$_2$] **1'** in $CDCl_3$−CS_2−DMSO-d_6.

^{13}C NMR spectrum (Fig. S5a) of C_{60}[>M(*t*-Bu)$_2$] **3** displaying one peak at δ 162.28 corresponding to the chemical shift of carbonyl carbon and 16 peaks in different intensities (14 peaks each with 2C and two peaks each with 1C) in the region of δ 135−150 that can be accounted for all 58 fullerenyl sp^2 carbons. The data is consistent with a C_{60} monoadduct structure having a C_{2v}-symmetrical ellipsoidal structure. Subsequent facile transesterification reaction of **3** with the well-characterized tertiary-amine precursor arm moiety, 4-hydroxy-[*N*,*N*',*N*,*N*,*N*,*N*-hexapropyl-hexa(aminoethyl) butanamide **5** ($C_3N_6C_3$-OH) afforded C_{60}[>M($C_3N_6^+C_3H$)$_2$] **6.** ^{13}C NMR spectrum of **6** (Fig. S5b) showed a total of 30 peaks (25 peaks each with 2C, 1 peak with 4C, and four peaks each with 1C) in the region of δ 135−150

accounted for 58 fullerenyl sp^2 carbons. The spectral data indicated clearly a C_2-symmetry of the compound **6**. Conversion of the compound **6** to $C_{60}[>M(C_3N_6^+C_3)_2]$ **1** was accompanied by multiple iodide anions. Unexpectedly, we were not able to detect any fullerenyl sp^2 carbon signals in the ^{13}C NMR spectrum of **1** under various deuterated solvent mixtures. However, these carbon signals re-appeared when all iodide anions were replaced by trifluoroacetate anions, leading to the corresponding salt **1'**. Accordingly, the ^{13}C NMR spectrum of **1'** (Fig. S5c) two peaks at δ 168.33 and 165.77 corresponding to the chemical shift of a carbonyl carbon of the amide (−HN-**C**=O) and the ester (−O-**C**=O) moieties, respectively. It also displayed a total of 30 peaks (25 peaks each with 2C, 1 peak with 4C, and four peaks each with 1C) in the region of δ 135−150 accounted for 58 fullerenyl sp^2 carbons, indicating a similar C_2-symmetry as that of the compound **6**

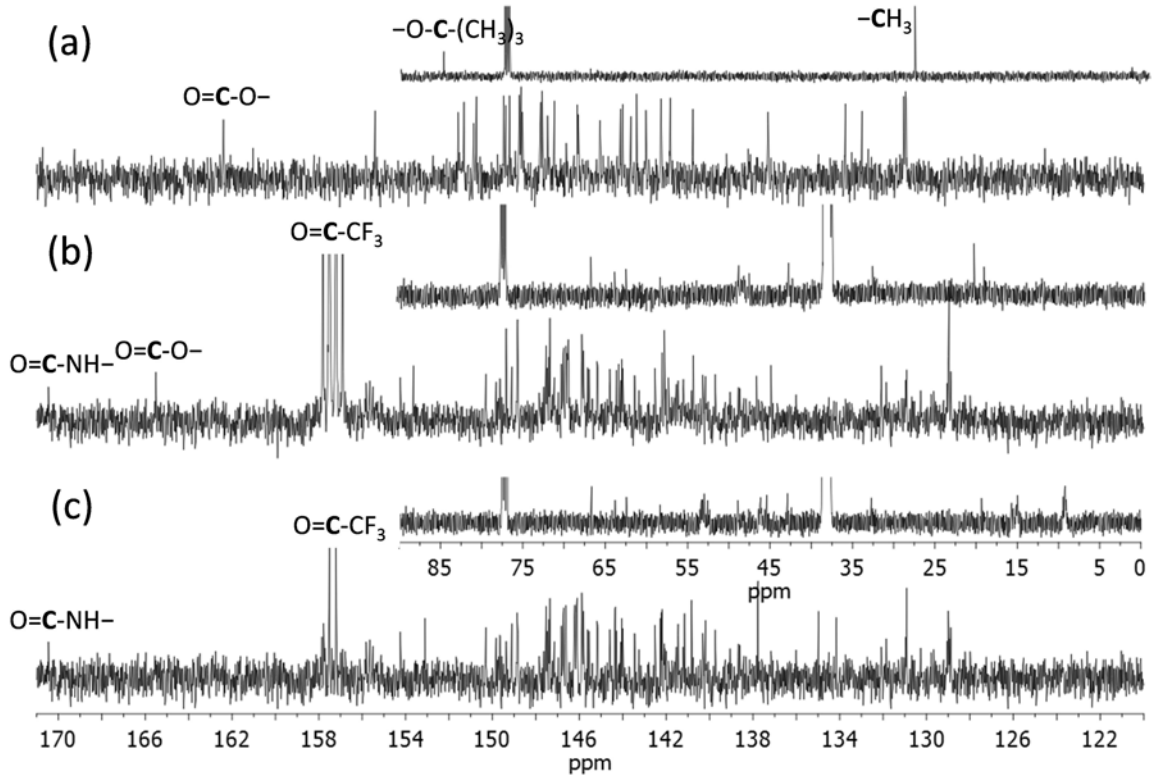

Figure S6. ^{13}C NMR spectra of (a) $C_{70}[>M(t\text{-}Bu)_2]$ **4** in $CDCl_3/CS_2$, (b) decacationic $C_{70}[>M(C_3N_6{}^+C_3H)_2]$ **7** in $CDCl_3/CS_2$/DMSO-d_6 , and (c) decacationic $C_{70}[>M(C_3N_6{}^+C_3)_2]$ **2'** in $CDCl_3/CS_2$/DMSO-d_6.

^{13}C NMR spectrum (Fig. S6a) of $C_{70}[>M(t\text{-}Bu)_2]$ **4** displaying one peak at δ 162.39 corresponding to the chemical shift of carbonyl carbon and 35 peaks in different intensities (33 peaks each with 2C and two peaks each with 1C) in the region of δ 125−155 that can be accounted for all 68 fullerenyl sp^2 carbons. The data is consistent with a C_{70} monoadduct structure having a C_s-symmetrical ellipsoidal structure with a plane of symmetry across the cyclopropane-bridged [6,6] bond. Subsequent facile transesterification reaction of **4** with the well-characterized tertiary-amine precursor arm moiety, 4-hydroxy-[*N*,*N*',*N*,*N*,*N*,*N*-hexapropyl-hexa(aminoethyl) butanamide **5** ($C_3N_6C_3$-OH) afforded $C_{70}[>M(C_3N_6{}^+C_3H)_2]$ **7.** ^{13}C NMR spectrum of **7** (Fig. S6b) showed two peaks at δ 170.45 and 165.50 corresponding to the

chemical shift of a carbonyl carbon of the amide (−HN-**C**=O) and the ester (−O-**C**=O) moieties, respectively. It also displayed a total of 68 peaks in the region of δ 125−155 accounted for 68 fullerenyl sp^2 carbons. The spectral data indicated clearly a C_1-symmetry of the compound **7**.

Conversion of the compound **7** to $C_{70}[>M(C_3N_6^+C_3)_2]$ **2**, was accompanied by multiple iodide anions. Unexpectedly, we were not able to detect any fullerenyl sp^2 carbon signals in the ^{13}C NMR spectrum of **2** under various deuterated solvent mixtures. However, these carbon signals re-appeared when all iodide anions were replaced by trifluoroacetate anions, leading to the corresponding salt **2'**. Accordingly, the ^{13}C NMR spectrum of **2'** (Fig. S6c) displayed a peak at δ 170.45 corresponding to the chemical shift of an amide carbonyl carbon (−HN-**C**=O), similar to that of **7**. It also displayed a total of 68 peaks in the region of δ 125−155 accounted for 68 fullerenyl sp^2 carbons, indicating a similar C_1-symmetry as that of the compound **7**.

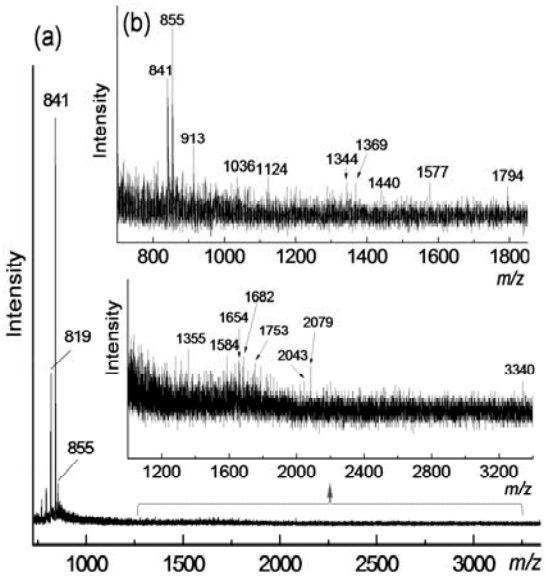

Figure S7. MALDI−TOF mass spectra (a) and (b) of decacationic $C_{70}[>M(C_3N_6^+C_3)_2]$ **2** under different laser intensity using sinapic acid as the matrix, showing molecular ion mass (M^+) at *m/z* 3340.

The mass spectroscopic data collection of $C_{70}[>M(C_3N_6^+C_3)_2]$ was proven to be difficult due to its polycationic nature and facile fragmentations occurring at the conjunction of the C_{70} cage and the decacationic malonate arm, giving mainly the highly detectable C_{70} ion mass at *m/z* 841, as displayed in MALDI−TOF mass spectra of Fig. S7. Fortunately, we are able to acquire several spectra in the high mass region showing the molecular ion mass (M^+) at *m/z* 3340 in low intensity accompanied with several identifiable fragmentation ion mass peaks at *m/z* 1355, 1584, 1654, 1682, 1753, 2043, and 2079. By variation of applied laser intensity, spectra containing many ion mass peaks in significant signal intensity in the medium mass region can be obtained, as shown in Fig. S7b. Structural elucidation of these ion fragments in the combined spectra of Figs. S7a and S7b allowed us to conclude a clear monoadduct structure of **2** by the sole detection of an ion fragment mass of $C_{70}(\text{-}CH_3)^+$ at *m/z* 855 without the corresponding ion fragment mass of the bisadduct $C_{70}(\text{-}CH_3)(>CH_2)^+$ at *m/z* 869. Analysis of the fragmentation pattern with a low peak intensity of nearly all mass ions at *m/z* >1000 indicated well with the bond cleavage occurring mostly at the cyclopropanyl carbon conjunction bonds bridging fullerene cage and 4-hydroxy-[*N*,*N*',*N*,*N*,*N*,*N*-hexapropyl-hexa(aminoethyl) butanamide arm moieties. We also observed a facile process of de-quaternization of **2** to its fragmented ions containing mostly tertiary hexa(alkylethylenylamino) arms under MALDI−MS conditions. Accordingly, we are able to elucidate the structure of monocationic mass fragments at *m/z* 1341, 1355, 1369, 1583, 1654, 1682, 1753, 1794, 2043, 2078, and 3349 with the latter as the molecular ion, as shown in Fig. S8. The structural pattern also revealed a faster bond cleavage of *n*-propyl group on the nitrogen atom than those of the methyl group and the main chain ethylenylamine moiety. These data strongly support the molecular mass of **2** as a $(C_3N_6^+C_3)_2$-malonate-C_{70} structure with many consistent $(C_3N_6C_n)_2$-malonate-C_{70} (C_n: methyl or *n*-propyl group) fragments.

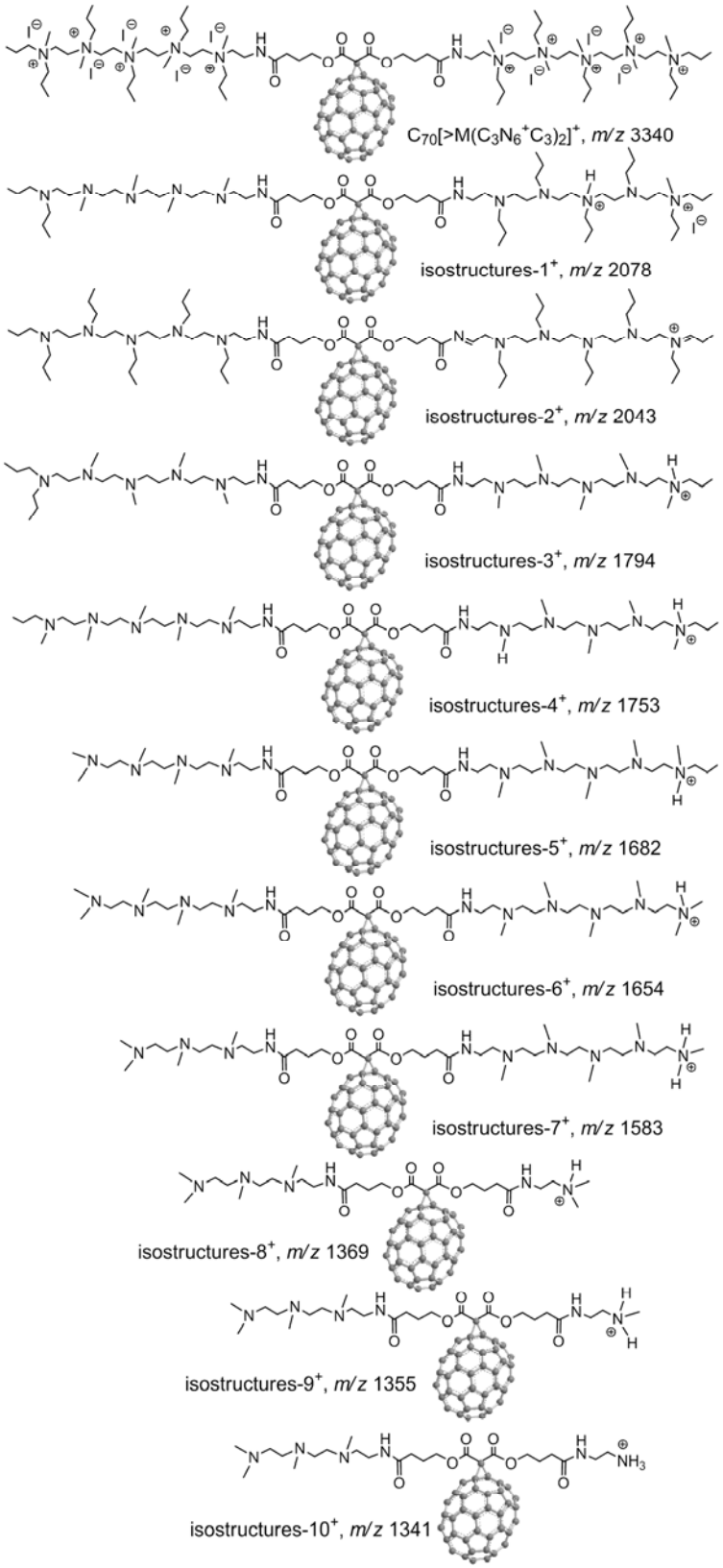

Figure S8. Structural elucidation of fragmented ion mass peaks in the MALDI−TOF mass spectra (Figures S7a and S7b) of $C_{70}[>M(C_3N_6^+C_3)_2]$ **2**.